XII International Conference on Computational Plasticity. Fundamentals and Applications
COMPLAS XII
E. Oñate, D.R.J. Owen, D. Peric and B. Suárez (Eds)

AN ADAPTIVE MULTI-LEVEL MODEL FOR MULTI-SCALE DUCTILE FRACTURE ANALYSIS IN HETEROGENEOUS ALUMINUM ALLOYS

DANIEL PAQUET* AND SOMNATH GHOSH†

* Research Scientist, Department of Metallurgy
Hydro-Québec Research Institute (IREQ)
1800 boul. Lionel-Boulet, Varennes, Québec J3X 1S1, Canada
e-mail: paquet.daniel@ireq.ca

†M. G. Callas Professor, Department of Civil Engineering
Johns Hopkins University
203 Latrobe, 3400 N. Charles Street, Baltimore, Maryland 21218, USA
e-mail: sghosh20@jhu.edu

Key words: Ductile Fracture, Aluminum Alloys, Multi-Scale Analysis, Homogenization, LE-VCFEM

Abstract. This paper addresses the multi-scale modeling of ductile fracture in microstructures characterized by a dispersion of hard and brittle heterogeneities in a softer ductile matrix. An adaptive multi-level model is developed with different inter-scale transfer operators and interfaces. Micro-mechanical analysis in regions of dominant damage is performed to capture the important micro-mechanical damage modes that are responsible for deterring the overall failure properties of these alloys. Regions of macroscopic homogeneity are otherwise modeled with constitutive relations derived from homogenization of evolving variables in representative volume elements. These two length scales of analysis, in conjunction with an intermediate swing level, form a three-level coupled multi-scale model to capture ductile crack propagation. The capabilities of the proposed model are demonstrated for a cast aluminum alloy.

1 INTRODUCTION

Over the past decades, several multi-scale models have been developed for predicting the overall mechanical behavior of multi-phase materials. Homogenization methods use asymptotic expansion to derive the macroscopic behavior of heterogeneous materials from representative volume element (RVE) boundary value problems. Linear (first-order homogenization) or higher-order kinematic variables are incrementally applied on the RVE boundary and the macroscopic stresses and state variables updated. While these methods

are successful for problems involving moderate gradients in macroscopic field variables, they fail to capture the localization of deformation and the micro-structural strain softening often associated with damage. Recently, more sophisticated methods have been developed to overcome this limitation. They are based on the partition of the RVE into two sub-domains, delineating the regions in which the material responses are stable and unstable. The homogenization method for the unstable sub-domain is specific to the type of damage considered and its accuracy strongly depends on the assumptions made in defining the equivalent discontinuity transferred to the macro-scale.

This paper proposes an alternative method in which micro-mechanical analysis is performed in regions of dominant damage, hence eliminating the need for homogenization in sub-domains with an unstable material response. An adaptive multi-level model for multi-scale analysis of ductile fracture in heterogeneous aluminum alloys has been developed by Ghosh and co-workers [1, 2, 3, 4, 5, 6, 7]. In this model, micro-mechanical analysis is performed in regions of intense damage with LE-VCFEM for ductile fracture [1, 2, 3], while macroscopic sub-domains are modeled with constitutive relations derived from homogenization [4, 5, 6]. These two levels of analysis in conjunction with an intermediate swing level form a three-level coupled multi-scale model to capture ductile crack propagation in multiple phase materials [7].

An overall description of the multi-level model developed in [1, 2, 3, 4, 5, 6, 7] for multi-scale analysis of ductile fracture is first presented in Section 2. Adaptivity criteria used for evolution of the multi-level model are detailed in Section 3, while the numerical scheme used to couple the different levels is addressed in Section 4. Finally, the capabilities of the proposed model are briefly illustrated in Section 5 for a cast aluminum microstructure.

2 LEVELS IN THE MULTI-SCALE MODEL

The multi-phase material computational domain Ω_{het} is adaptively decomposed into a set of non-intersecting sub-domains, denoted by *level-0*, *level-1*, *level-2*, and *level-tr*, i.e. $\Omega_{het} = \Omega_{l0} \cup \Omega_{l1} \cup \Omega_{l2} \cup \Omega_{tr}$. The different levels of computational hierarchy are depicted in Figure 1 and follow the nomenclature adopted in [8] for multi-scale analysis of microstructurally debonding composites. Concurrent multi-scale analysis requires that all levels be coupled for simultaneous solving of variables in the different sub-domains. The algorithmic treatments corresponding to each level, in order of emergence, are discussed briefly in the following.

2.1 Computational sub-domain *level-0* (Ω_{l0})

In sub-domain Ω_{l0}, macroscopic computations are executed using traditional finite element method (FEM) algorithms. In order to capture the effect of the microstructure and its evolution, the continuum constitutive models used in the analysis are obtained by homogenizing the material response in a microstructural RVE.

A micrograph of cast aluminum alloy W319, studied in this paper, and the corre-

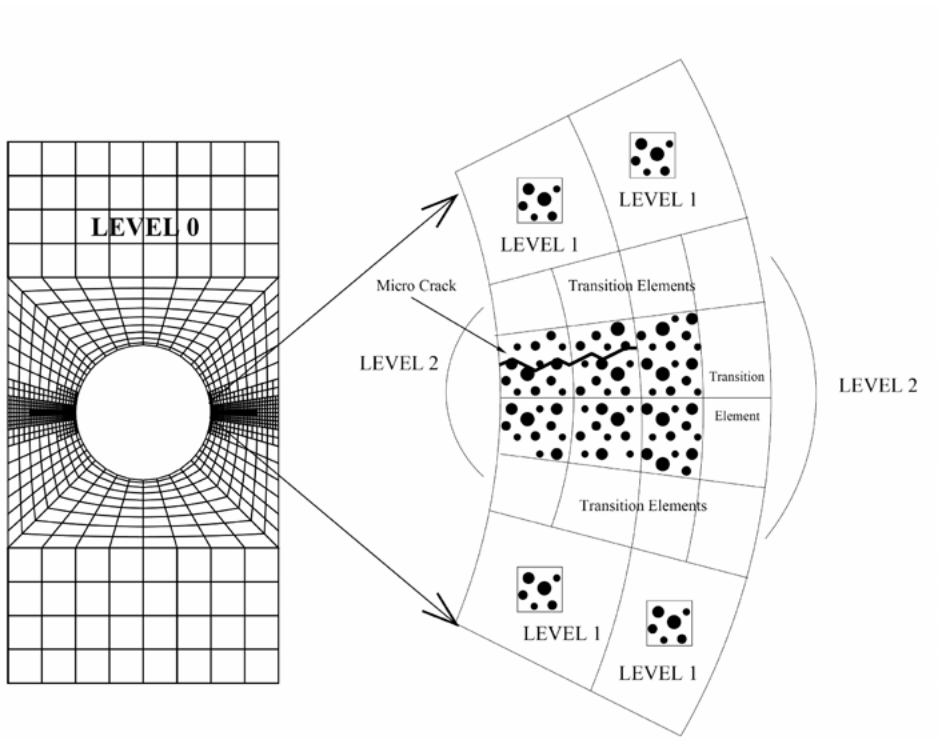

Figure 1: Schematic of a coupled concurrent multi-level model showing: (left) *level-0* region of macroscopic continuum analysis with adaptive mesh refinement and (right) blow-up of critical region surrounding a crack containing *level-1* and *level-2* regions of analyses.

sponding RVE are shown in Figure 2. The microstructure of this alloy is characterized by a dispersion of brittle silicon (Si) inclusions in an age-hardened aluminum matrix. Rate-independent and rate-dependent homogenization-based continuum plasticity-damage (HCPD) models have been developed for macroscopic analysis of diffuse deformation and damage in porous ductile materials containing brittle inclusions. A complete description of those macroscopic models can be found in [4, 5, 6].

2.2 Computational sub-domain *level-1* (Ω_{l1})

Computational sub-domain Ω_{l1} is used to identify the regions requiring switching over from macroscopic to microscopic computations. Macroscopic analysis is valid in Ω_{l1}, but the intensity of field variables and their gradients indicates an eminent departure from homogeneity.

Two analyses are required for this sub-domain. A macroscopic analysis based on the HCPD model is first performed and the macroscopic fields are updated. Then follows a LE-VCFEM [1, 2, 3] based micro-mechanical analysis of the microstructural RVE with periodicity boundary conditions and applied strain tensor obtained from the macroscopic analysis [6]. A criterion based on the microstructural response of the RVE is then used

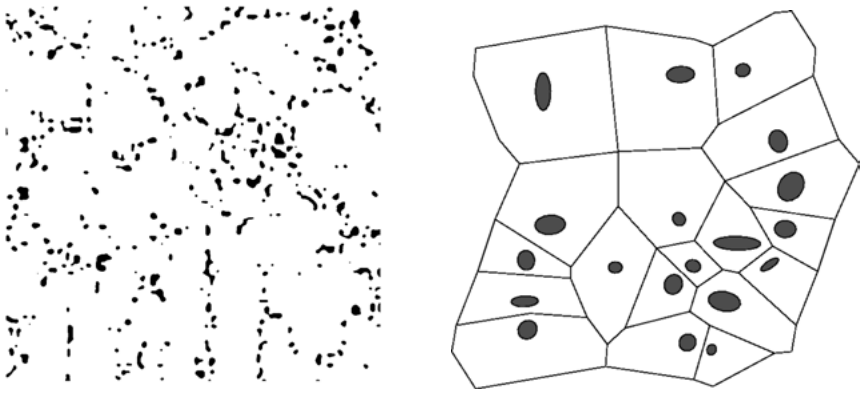

(a) (b)

Figure 2: (a) Micrograph of a cast aluminum alloy W319 (192μm x 192μm) and (b) RVE of the microstructure in (a) (48μm x 48μm) (Micrograph: Courtesy Ford Research Laboratory).

to indicate transition from *level-1* to *level-2* elements.

2.3 Computational sub-domain *level-2* (Ω_{l2})

Microscopic sub-domain Ω_{l2} emerges from *level-1* elements for which detailed micro-mechanical analysis is needed. This sub-domain incorporates the morphology of the underlying microstructure and is solved with LE-VCFEM for ductile fracture [1, 2, 3]. This method uses information on microstructural morphology and the computational efforts required for the micro-mechanical analysis are significantly reduced.

2.4 Transition interface layer (Ω_{tr})

Elements in Ω_{tr} are *level-2* elements that have compatibility and traction continuity constraints imposed on their interface with the macroscopic sub-domain $\Omega_{l0} \cup \Omega_{l1}$. They are located beyond the *level-2* regions and are introduced to regularize kinetic and kinematic incompatibilities at the interface using a relaxed displacement constraint method. Numerical implementation of this method using Lagrange multipliers technique is addressed in Section 4.

3 MESH REFINEMENT AND LEVEL CHANGE CRITERIA

Implementation of the multi-level model requires appropriate criteria for mesh refinement and level changes [7]. These criteria are briefly discussed next.

3.1 Mesh refinement in Ω_{l0}

Discretization errors in Ω_{l0} are minimized by an h-adaptation mesh refinement strategy. The adaptation criterion is formulated in terms of traction jumps across adjacent element boundaries. An element e in Ω_{l0} is subdivided into smaller elements if the following

condition is satisfied:

$$E_e^{tj} \geq C_1 E_{max}^{tj} \quad \text{with} \quad E_e^{tj} = \sqrt{\frac{\int_{\partial\Omega_e}([[t_x]]^2 + [[t_y]]^2) d\partial\Omega}{\int_{\partial\Omega_e} d\partial\Omega}} \tag{1}$$

where E_{max}^{tj} is the highest value of all E_e^{tj} for all *level-0* elements in Ω_{l0} and $C_1 < 1$ is a prescribed factor chosen from numerical experiments. In criterion (1), t_x and t_y are the boundary traction components in x and y directions and $[[\cdot]]$ is the jump operator across the element boundary $\partial\Omega_e$.

3.2 Criterion for switching from *level-0* to *level-1* elements

Departure from homogenizability in ductile materials occurs in regions characterized by a localization of damage due to void nucleation and growth. Hence, a criterion combining macroscopic void volume fraction $\bar{f}$ and its gradients is used for conditioning the transition from *level-0* to *level-1* elements:

$$E_e^{gdf} f_e^\star \geq C_2 E_{max}^{gdf} f_{max}^\star \quad \text{with} \quad E_e^{gdf} = \sqrt{\frac{\partial {f_e^\star}^2}{\partial x} + \frac{\partial {f_e^\star}^2}{\partial y}} \tag{2}$$

where $f^\star = \frac{\bar{f} - \bar{f}_0}{\bar{f}_0}$ is the normalized void volume fraction with respect to the initial void volume fraction $\bar{f}_0$, and $f_{max}^\star$ and E_{max}^{gdf} are the maximum values of all $f_e^\star$ and E_e^{gdf} respectively. The factor $C_2 < 1$ is determined from numerical experiments.

3.3 Criterion for switching from *level-1* to *level-2* elements

Transition from *level-1* to *level-2* is activated for elements in Ω_{l1} for which RVE periodicity is violated. Since periodic displacement boundary conditions are applied on the RVE (cf. Section 2.2), violation of traction anti-periodicity on the RVE boundary is used to trigger the transition. An element e in Ω_{l1} is switched to Ω_{l2} if the following criterion is met:

$$TR_e^{apt} \geq C_3 \quad \text{with} \quad TR_e^{apt} = \frac{\left|\left|\sum_{i=1}^{NSGPR} \int_{\Gamma_i} \left(\left|t_x^{i+} + t_x^{i-}\right| \mathbf{i} + \left|t_y^{i+} + t_y^{i-}\right| \mathbf{j} \right) d\Gamma \right|\right|}{\max_e \left|\left|\sum_{i=1}^{NSEG} \int_{\Gamma_i} \left(\left|t_x^{i}\right| \mathbf{i} + \left|t_y^{i}\right| \mathbf{j} \right) d\Gamma \right|\right|} \tag{3}$$

where TR_e^{apt} is a measure of the lack of anti-periodicity of boundary tractions and $C_3 < 1$. $NSGPR$ is the number of boundary segment-pairs on the boundary of each RVE (e.g. Figure 2(b)) and $NSEG$ is the total number of segments on the RVE boundary. Superscripts + and - in equation (3) correspond to the tractions on the segment pairs with anti-periodicity conditions. The numerator is a measure of the residual traction violating the anti-periodicity condition. The denominator on the other hand corresponds to the

maximum value of the absolute sum of all traction measures in all the RVEs of *level-1* elements. $TR_e^{apt} = 0$ indicates a perfect anti-periodicity of boundary tractions.

The microstructural information within each newly created *level-2* element is updated using the history of the macroscopic displacement solution on the macroscopic element boundary. A relaxation step is also performed to recover local equilibrium after connecting the newly created *level-2* element to the multi-scale mesh.

4 COUPLING MULTIPLE LEVELS FOR MULTI-SCALE ANALYSIS

Multi-scale analysis requires that all levels be coupled and solved simultaneously in sub-domains Ω_{l0}, Ω_{l1}, Ω_{l2}, and Ω_{tr}. The global stiffness matrix and load vectors are derived for the entire computational domain $\Omega_{het} = \Omega_{l0} \cup \Omega_{l1} \cup \Omega_{l2} \cup \Omega_{tr}$. The corresponding domain boundary is partitioned as $\Gamma_{het} = \Gamma_{l0} \cup \Gamma_{l1} \cup \Gamma_{l2} \cup \Gamma_{tr}$, where $\Gamma_{l0} = \Gamma_{het} \cap \partial\Omega_{l0}$, $\Gamma_{l1} = \Gamma_{het} \cap \partial\Omega_{l1}$, $\Gamma_{l2} = \Gamma_{het} \cap \partial\Omega_{l2}$, and $\Gamma_{tr} = \Gamma_{het} \cap \partial\Omega_{tr}$. The interface between these two modeling scales is denoted $\Gamma_{int} = (\partial\Omega_{l0} \cup \partial\Omega_{l1}) \cap (\partial\Omega_{l2} \cup \partial\Omega_{tr})$. Displacement continuity and traction reciprocity at the interface between the macro-scale sub-domain $\Omega_{l0} \cup \Omega_{l1}$ and micro-scale sub-domain $\Omega_{l2} \cup \Omega_{tr}$ are enforced (in a weak sense) with the relaxed displacement constraint method [7].

4.1 Weak form for the multi-level multi-scale model

The principle of virtual work for Ω_{het} at the end of the increment $n+1$, associated with a virtual displacement field δu_i, is expressed as follows [7]:

$$\delta\Pi_{het}^{n+1} = \delta\Pi_{\Omega_{l0}}^{n+1} + \delta\Pi_{\Omega_{l1}}^{n+1} + \delta\Pi_{\Omega_{l2}}^{n+1} + \delta\Pi_{\Omega_{tr}}^{n+1} + \delta\Pi_{\Gamma_{int}}^{n+1} = 0 \tag{4}$$

where the individual contributions from each sub-domain are defined as follows:

$$\begin{aligned}
\delta\Pi_{\Omega_{l0}}^{n+1} &= \int_{\Omega_{l0}} (\Sigma_{ij}^{l0} + \Delta\Sigma_{ij}^{l0}) \frac{\partial \delta u_i^{l0}}{\partial x_j} d\Omega - \int_{\Gamma_{l0}} (t_i^{l0} + \Delta t_i^{l0}) \delta u_i^{l0} d\Gamma \\
\delta\Pi_{\Omega_{l1}}^{n+1} &= \int_{\Omega_{l1}} (\Sigma_{ij}^{l1} + \Delta\Sigma_{ij}^{l1}) \frac{\partial \delta u_i^{l1}}{\partial x_j} d\Omega - \int_{\Gamma_{l1}} (t_i^{l1} + \Delta t_i^{l1}) \delta u_i^{l1} d\Gamma \\
\delta\Pi_{\Omega_{l2}}^{n+1} &= \int_{\Omega_{l2}} (\sigma_{ij}^{l2} + \Delta\sigma_{ij}^{l2}) \frac{\partial \delta u_i^{l2}}{\partial x_j} d\Omega - \int_{\Gamma_{l2}} (t_i^{l2} + \Delta t_i^{l2}) \delta u_i^{l2} d\Gamma \\
\delta\Pi_{\Omega_{tr}}^{n+1} &= \int_{\Omega_{tr}} (\sigma_{ij}^{tr} + \Delta\sigma_{ij}^{tr}) \frac{\partial \delta u_i^{tr}}{\partial x_j} d\Omega - \int_{\Gamma_{tr}} (t_i^{tr} + \Delta t_i^{tr}) \delta u_i^{tr} d\Gamma \\
\delta\Pi_{\Gamma_{int}}^{n+1} &= \delta \int_{\Gamma_{int}} (\lambda_i^{l0/l1} + \Delta\lambda_i^{l0/l1})(v_i + \Delta v_i - u_i^{l0/l1} - \Delta u_i^{l0/l1}) d\Gamma \\
&+ \delta \int_{\Gamma_{int}} (\lambda_i^{tr} + \Delta\lambda_i^{tr})(v_i + \Delta v_i - u_i^{tr} - \Delta u_i^{tr}) d\Gamma
\end{aligned}$$

Superscripts $l0$, $l1$, $l2$, and tr in equation (4) relate the variables to their respective sub-domain. Variables in $\delta\Pi_{het}^{n+1}$ are evaluated at the end of the increment $n+1$, i.e.

$(\cdot)^{n+1} = (\cdot)^n + (\Delta\cdot)^{n+1}$. Superscripts n and $n+1$ are dropped in equation (4) for sake of clarity.

The last term in equation (4) couples macro-scale stresses $\Sigma_{ij}^{l0/l1}$, tractions $t_i^{l0/l1}$ and displacements $u_i^{l0/l1}$ with their micro-scale counter parts $\sigma_{ij}^{l2/tr}$, $t_i^{l2/tr}$ and $u_i^{l2/tr}$. For this, the displacement field v_i is interpolated on each segment of the interface Γ_{int} using a suitable polynomial function, independent of the interpolations on $\partial\Omega_{l0}$, $\partial\Omega_{l1}$, $\partial\Omega_{l2}$, and $\partial\Omega_{tr}$. Lagrange multipliers $\lambda_i^{l0/l1}$ and λ_i^{tr} are then introduced in $\delta\Pi_{\Gamma_{int}}^{n+1}$ to enforce displacement continuity and traction reciprocity at the interface (in a week sense). Hence, setting the coefficients of $\delta\lambda_i^{l0/l1}$ and $\delta\lambda_i^{tr}$ to zero leads to the following Euler equations:

$$\begin{array}{rcll} u_i^{l0/l1} + \Delta u_i^{l0/l1} & = & v_i + \Delta v_i & \\ u_i^{tr} + \Delta u_i^{tr} & = & v_i + \Delta v_i & \text{on } \Gamma_{int} \end{array} \tag{5}$$

These correspond to displacement continuity across Γ_{int}. Traction reciprocity across Γ_{int} results from setting the coefficients of δv_i, $\delta u_i^{l0/l1}$, and δu_i^{tr} to zero:

$$\begin{array}{rcll} \lambda_i^{l0/l1} + \Delta\lambda_i^{l0/l1} & = & -(\lambda_i^{tr} + \Delta\lambda_i^{tr}) & \\ \lambda_i^{l0/l1} + \Delta\lambda_i^{l0/l1} & = & (\Sigma_{ij}^{l0/l1} + \Delta\Sigma_{ij}^{l0/l1}) n_j^{l0/l1} & \text{on } \Gamma_{int} \\ \lambda_i^{tr} + \Delta\lambda_i^{tr} & = & (\sigma_{ij}^{tr} + \Delta\sigma_{ij}^{tr}) n_j^{tr} & \end{array} \tag{6}$$

where n_j is the unit normal vector and $\lambda_i^{l0/l1}$ and λ_i^{tr} correspond to the interfacial traction (in a week sense) on $\partial\Omega_{l0/l1} \cap \Gamma_{int}$ and $\partial\Omega_{tr} \cap \Gamma_{int}$ respectively. The other Euler relations obtained by setting the coefficients of $\delta u_i^{l0/l1}$ and $\delta u_i^{l2/tr}$ to zero are the equilibrium equations in each sub-domains and different traction reciprocity conditions between the sub-domains.

4.2 Finite element discretization

Macro-scale displacements $u_i^{l0/l1}$ in each *level-0* and *level-1* elements are interpolated with standard shape functions as:

$$\{\mathbf{u}^{l0/l1}\} = [\mathbf{N}_{l0/l1}]\{\mathbf{q}_{l0/l1}\} = [\mathbf{N}_{l0/l1}^I \ \mathbf{N}_{l0/l1}^O] \begin{Bmatrix} \mathbf{q}_{l0/l1}^I \\ \mathbf{q}_{l0/l1}^O \end{Bmatrix} \tag{7}$$

where the nodal displacements are partitioned into two sets, viz. the nodes $\mathbf{q}_{l0/l1}^I$ lying on the interface Γ_{int} and the other degrees of freedom $\mathbf{q}_{l0/l1}^O$.

At the interface Γ_{int}, displacements v_i and Lagrange multipliers $\lambda_i^{l0/l1}$ and λ_i^{tr} are interpolated from nodal values using suitable shape functions:

$$\{\mathbf{v}\} = [\mathbf{L}_{int}]\{\mathbf{q}_{int}\} \tag{8}$$

$$\{\boldsymbol{\lambda}^{l0/l1}\} = [\mathbf{L}_{\lambda^{l0/l1}}]\{\boldsymbol{\Lambda}_{l0/l1}\} \tag{9}$$

$$\{\boldsymbol{\lambda}^{tr}\} = [\mathbf{L}_{\lambda^{tr}}]\{\boldsymbol{\Lambda}_{tr}\} \tag{10}$$

Spurious stress concentrations at the interface are avoided with a proper choice of shape functions in equations (8)-(10) [7].

An iterative solver is used to solve the nonlinear equations obtained by setting the residual $\mathbf{R}$ in equation (4) to zero. Setting up the stiffness matrix $\frac{\partial \mathbf{R}}{\partial q_i}$, where q_i comprises all the degrees of freedom in equations (7)-(10), requires consistent linearization by taking directional derivatives of equation (4) along incremental displacement vectors $\Delta\mathbf{u}$ and $\Delta\mathbf{v}$, and the Lagrange multipliers $\Delta\boldsymbol{\lambda}$. Especially, the stiffness sub-matrix and load sub-vector associated with *level-2* and *level-tr* elements are obtained from LE-VCFEM calculations followed by a static condensation to retain the boundary terms only. More details on the numerical implementation of the multi-level multi-scale model can be found in [7].

5 APPLICATION TO A CAST ALUMINUM MICROSTRUCTURE

This numerical example studies the microstructural response of a cast aluminum alloy when submitted to an applied homogeneous traction. Details on the computational domain and on the modeling parameters are given, and the numerical results discussed. A complete description of the numerical problem can be found in [7].

5.1 Computational domain

The microstructure analyzed in this example was extracted from a micrograph of a cast aluminum alloy W319 used in the automotive industry (cf. Figure 2(a)). The dimensions of the rectangular computational domain are $384\mu\text{m} \times 1536\mu\text{m}$ in the horizontal (x) and vertical (y) directions respectively. This tensile specimen is discretized into $8 \times 32 = 256$ macro-scale elements, each of which has dimensions $48\mu\text{m} \times 48\mu\text{m}$. Prescribed boundary conditions are: (i) $u_y = U$ at $y = 1536\mu\text{m}$, (ii) $u_y = 0$ at $y = 0$, and (iii) $u_x = 0$ at $(x, y) = (0, 0)$.

Prior to the multi-scale analysis, the results of the sensitivity analysis in [1, 2] are used to identify the macros-scale elements, among the 256, that are prone to ductile fracture. These critical regions are characterized by higher values of inclusion volume fraction and inclusion clustering. Based on the results, six critical regions are identified for which LE-VCFEM micro-mechanical analysis will be performed from the beginning of the multi-scale simulation. Once the critical regions Ω_{l2} identified, the remaining elements are merged to form a macroscopic sub-domain Ω_{l0}. This leads to the initial mesh for the multi-scale analysis shown in Figure 3(a).

5.2 Modeling parameters

The inclusion and matrix constitutive relations and material parameters used for LE-VCFEM micro-mechanical analysis are reported in [7]. An RVE size $L_{RVE} = 48\mu\text{m}$

was derived from a statistical analysis of the microstructure [6] and the RVE used for calibrating the macroscopic material parameters is shown in Figure 2(b). Details on the HCPD model constitutive relations and the procedure developed for the calibration of material parameters are given in [7, 4, 5, 6].

The parameters in equations (2) and (3) used for level change conditioning are $C_2 = 0.2$ and $C_3 = 0.1$. Adaptive mesh refinement is not considered because the macro-scale elements have the same dimensions as the size of the RVE.

5.3 Numerical results

Upon loading, inclusion cracking and matrix deformation generate non-uniformities in the microscopic sub-domain Ω_{l2}. Macroscopic deformation and damage localize in neighboring *level-0* elements and transition to Ω_{l1} sub-domain is activated when loss of macroscopic homogeneity is detected. The microscopic sub-domain Ω_{l2} subsequently propagates in regions of Ω_{l1} for which RVE periodicity is violated. This adaptive evolution of the multi-level mesh, following the formation and growth of a macroscopic ductile crack, is shown in Figure 3.

Three of the initial microscopic sub-domains propagate and merge to form a dominant macroscopic damage zone (Figure 3(a)-(f)). The microscopic sub-domain Ω_{l2} then stabilizes until localization of damage within a *level-2* microstructure leads to its complete failure. At total failure, the *level-2* element is replaced or "sealed" by a macroscopic element (black elements in Figure 3) with near-zero constant stresses.

Element sealing occurs for the first time at an applied displacement $U = 13.2\mu$m. A contour plot of microscopic void volume fraction after failure of the *level-2* element is given in Figure 4(a), showing a distinct ductile crack in its microstructure. Plot of microscopic stress σ_{yy} at the onset of local failure and the underlying microstructure of the Ω_{l2} sub-domain are also shown in Figure 4.

This failure process continues until the macro-crack becomes extremely unstable and final failure of the structure occurs.

6 CONCLUSIONS

- The concurrent multi-level model presented in this paper was developed to capture damage phenomena such as deformation localization and strain softening.

- LE-VCFEM based micro-mechanical analyses are performed in regions with unstable material response, eliminating the need for homogenization in those regions.

- Homogenization-based plasticity-damage (HCPD) models are used in regions of macroscopic homogenizability. These models are derived from homogenization of evolving variables in microstructural RVE and incorporate important microstructural morphology information.

- A third level of analysis is added as an intermediate swing level to form a three-level coupled multi-scale model to capture ductile crack propagation. Transition from macroscopic to microscopic analysis is established by a criterion quantifying the lack of anti-periodicity of RVE boundary tractions.

- The proposed multi-scale model successfully captures detailed microscopic fracture in a large material microstructure with minimal computational resources by an adaptive propagation of microstructural sub-domains, following microstructural damage evolution from initiation to final failure.

REFERENCES

[1] Paquet, D. and Ghosh, S. Microstructural effects on ductile fracture in heterogeneous materials. Part I: Sensitivity analysis with LE-VCFEM. *Eng. Fract. Mech.* (2011) **78**:205–225.

[2] Paquet, D. and Ghosh, S. Microstructural effects on ductile fracture in heterogeneous materials. Part II: Application to cast aluminum microstructures. *Eng. Fract. Mech.* (2011) **78**:226–233.

[3] Hu, C. and Ghosh, S. Locally enhanced Voronoi cell finite element model (LE-VCFEM) for simulating evolving fracture in ductile microstructures containing inclusions. *Int. J. Numer. Methods Engrg* (2008) **76**:1955–1992.

[4] Dondeti, P., Paquet, D. and Ghosh, S. A rate-dependent homogenization based continuum plasticity-damage (HCPD) model for dendritic cast aluminum alloys. *Eng. Fract. Mech.* (2012) **89**:75–97.

[5] Paquet, D., Dondeti, P. and Ghosh, S. Dual-stage nested homogenization for rate-dependent anisotropic elasto-plasticity model of dendritic cast aluminum alloys. *Int. J. Plasticity* (2011) **27**:1677–1701.

[6] Ghosh, S., Bai, J. and Paquet, D. Homogenization-based continuum plasticity-damage model for ductile failure of materials containing heterogeneities. *J. Mech. Phys. Solids* (2009) **57**:1017–1044.

[7] Ghosh, S. and Paquet, D. Adaptive concurrent multi-level model for multi-scale analysis of ductile fracture in heterogeneous aluminum alloys. *Submitted for publication.*

[8] Ghosh, S., Bai, J. and Raghavan, P. Concurrent multi-level model for damage evolution in microstructurally debonding composites. *Mech. Mater.* (2007) **39**:241–266.

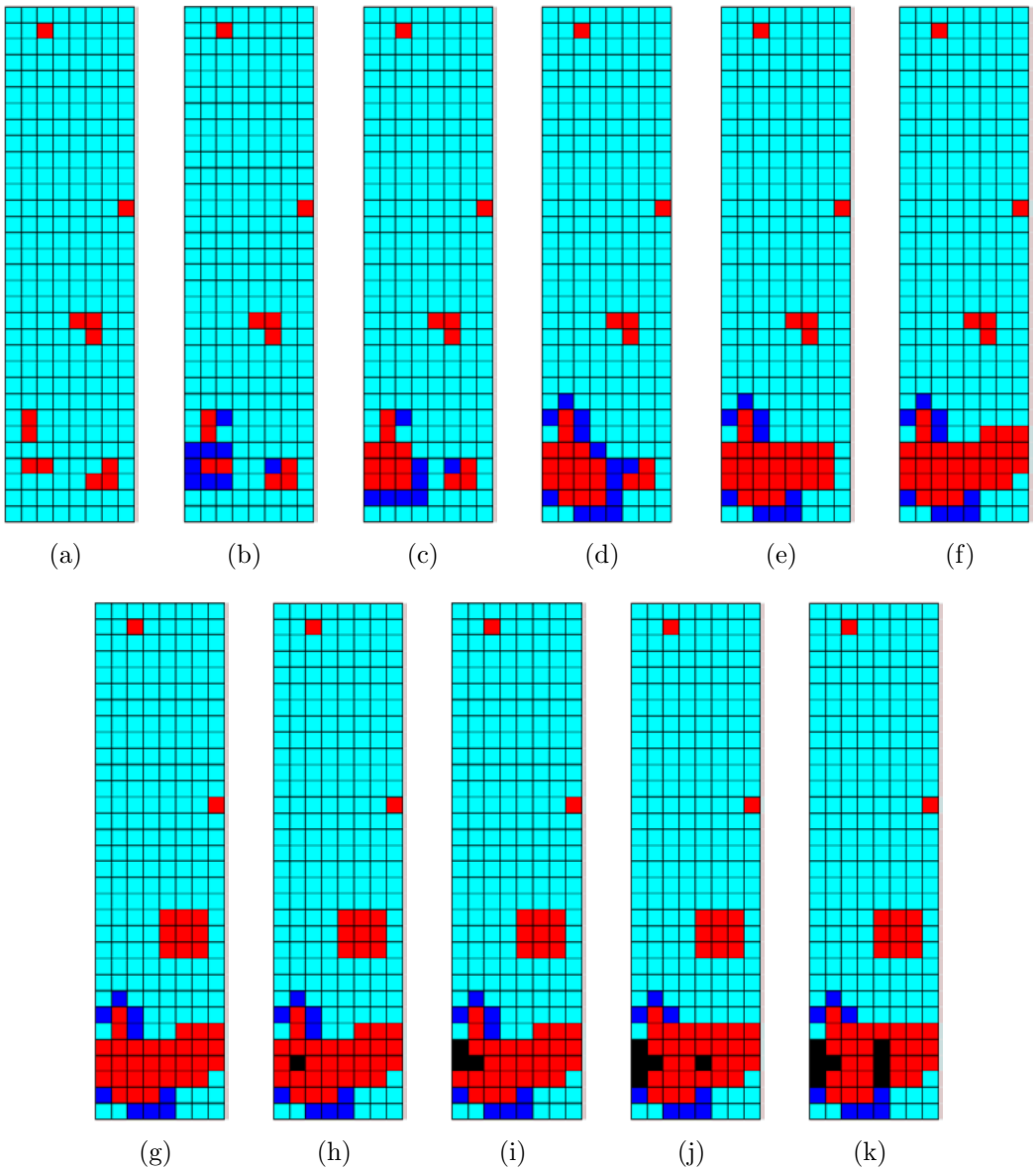

Figure 3: Evolution of the adaptive multi-level mesh during the multi-scale analysis: (a) $U = 0$, (b) $U = 7.4\mu$m, (c) $U = 7.6\mu$m, (d) $U = 7.8\mu$m, (e) $U = 10.1\mu$m, (f) $U = 10.3\mu$m, (g) $U = 13.0\mu$m, (h) $U = 13.2\mu$m, (i) $U = 13.3\mu$m, (j) $U = 13.5\mu$m, and (k) $U = 13.7\mu$m. (Legend: *level-0* (turquoise), *level-1* (blue), *level-2/tr* (red), sealed elements (black)).

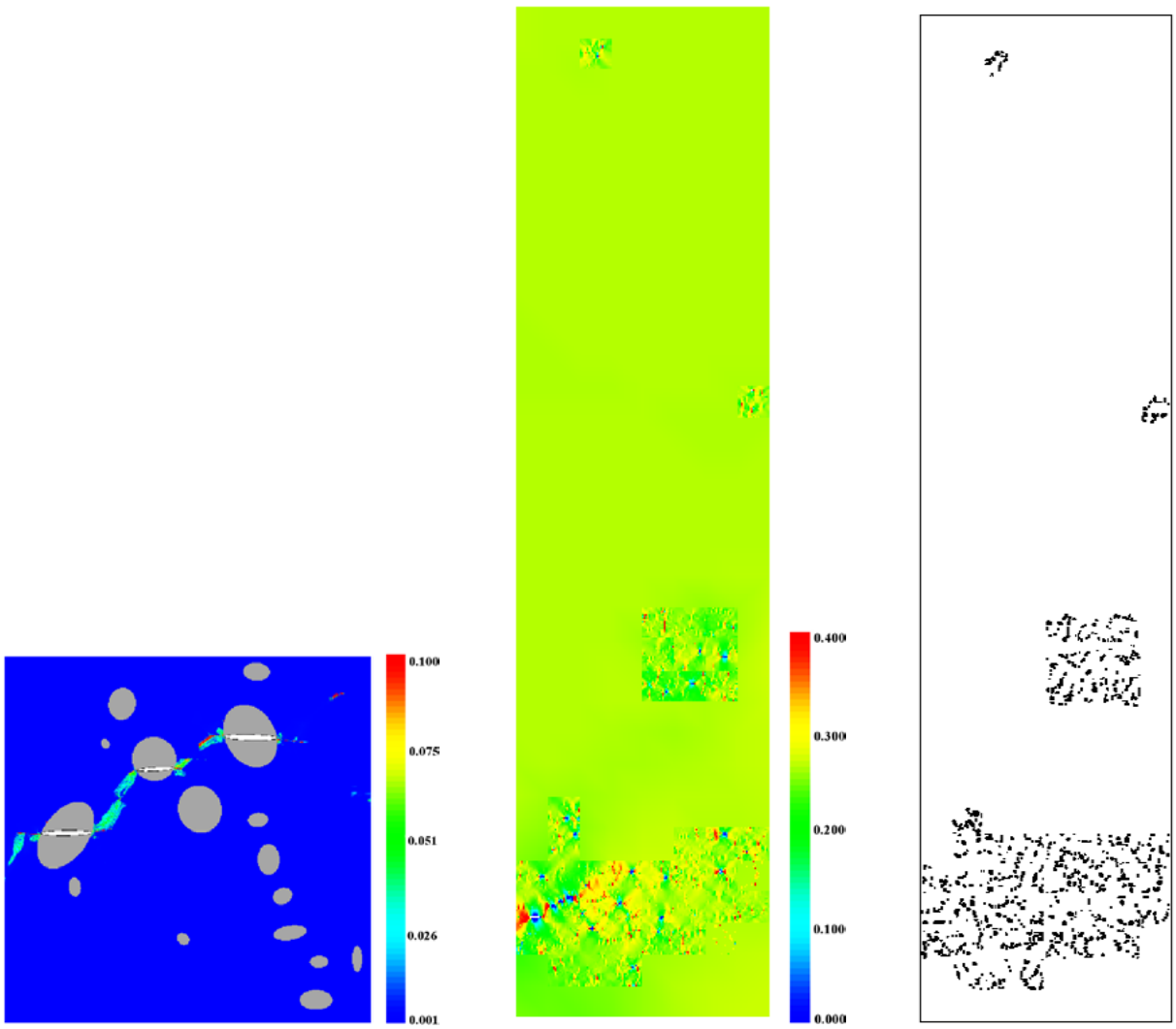

(a) (b) (c)

Figure 4: (a) Contour plot of void volume fraction f showing the final crack path after complete failure of the first *level-2* element sealed during the multi-scale simulation, (b) contour plot of microscopic stress component σ_{yy} (GPa) for the entire computational domain of the tensile specimen at an applied displacement $U = 13.0\mu$m, and (c) underlying microstructure of the *level-2* elements of the adaptive multi-level mesh.